Computer Aided Study of the Ranque–Hilsch Vortex Tube Using Advanced Three-Dimensional Computational Fluid Dynamics Software

RONÁN OLIVER, FERGAL BOYLE, ANTHONY REYNOLDS
Department of Mechanical Engineering
Dublin Institute of Technology
Bolton St., Dublin 1
IRELAND

Abstract: In this investigation the highly-complex, compressible, swirling, and turbulent flow within a Ranque–Hilsch vortex tube has been captured in a three dimensional flow domain using the state-of-the-art ANSYS CFX™ Computational Fluid Dynamic software package. These results have also been successfully compared to vortex tube configurations for which reliable experimental results exist. Additionally a mesh convergence study focusing on the cold temperature output of the vortex tube has been conducted.

Key – Words: Ranque-Hilsch Vortex Tube, Primary and Secondary Flow, Computational Fluid Dynamics.

1 Introduction

The Ranque-Hilsch Vortex Tube (RHVT) is an ingenious invention credited to both Georges Joseph Ranque and Rudolf Hilsch, who contrived the device independently during war torn Europe in the 1940's [1].

A RHVT separates an injected stream of gas into two streams, one significantly hotter along with another substantially colder than the injected stream. This is remarkable considering the absence of any moving parts or work input. While geometrically simple, the fluid dynamic and thermodynamic processes in a RHVT are extremely complex. To experimentally measure and plot velocity, pressure and temperature contours accurately within the tube in order to gain a better insight into the mode of heat migration is very difficult. A simpler alternative is to employ Computational Fluid Dynamics (CFD). Currently there is no conclusive evidence as to the mode of energy migration within the RHVT.

In this CFD study of the RHVT, the flow fields and temperature outputs have been investigated. This study began with the appropriate selection of experimental results from a range of authors for similar vortex tubes. Once these results were collated a three dimensional model of a similar experimental RHVT was drawn, upon which an unstructured tetrahedral mesh has been developed using the CAD and meshing facilities of the CFD package respectively. This model was developed in such a way so as components of the RHVT could be easily adjusted in size in order to carry out small scale parametric studies of the vortex tube. The analysis then moved on to the correct stipulation of suitable and accurate boundary conditions. Once a set of appropriate and realistic boundary conditions were established the flow fields within the RHVT were captured. These flow fields have been compared to the experimental results and are proven to be accurate. Additionally a mesh element density convergence study of the cold static and total temperature outputs of the RHVT has been examined in detail.

2 Computational Fluid Dynamics

CFD is the process whereby numerical methods are employed to simulate real-life fluid flows. CFD is now regarded as the "third" technique for the solution of fluid flow problems, complementing, but not replacing, the well-established approaches of theory and experiment. It is a relatively new branch of fluid mechanics and finds its niche in predicting fluid flows that are difficult or impossible to analyse using theory and are complex, time consuming, or expensive to measure experimentally.

2.1 Governing Equations of Fluid Dynamics

In understanding how CFD works, it must be borne in mind that the governing equations of fluid mechanics are fundamental to CFD. In CFD literature, the complete form of the time averaged equations governing fluid motion is referred to as the Reynolds-Averaged Navier-Stokes equations. Letting ρ, $\mathbf{U}$, u, v, w, P, and E denote density, the velocity vector, the x, y and z mean components of the velocity vector, static pressure and total energy per unit volume respectively, the final form of these

Reynolds-Averaged Navier-Stokes equations is as follows:

$$\frac{\partial \rho}{\partial t} + \nabla.(\rho \mathbf{U}) = 0 \quad (1)$$

$$\frac{\partial \rho u}{\partial t} + \nabla.(\rho u \mathbf{U}) = -\frac{\partial P}{\partial x} + \nabla.(\mu \nabla \mathrm{u}) - \frac{\partial\left(\rho \overline{u'^2}\right)}{\partial x} - \frac{\partial\left(\rho \overline{u'v'}\right)}{\partial y} - \frac{\partial\left(\rho \overline{u'w'}\right)}{\partial z} \quad (2)$$

$$\frac{\partial \rho v}{\partial t} + \nabla.(\rho v \mathbf{U}) = -\frac{\partial P}{\partial y} + \nabla.(\mu \nabla v) - \frac{\partial\left(\rho \overline{u'v'}\right)}{\partial x} - \frac{\partial\left(\rho \overline{v'^2}\right)}{\partial y} - \frac{\partial\left(\rho \overline{v'w'}\right)}{\partial z} \quad (3)$$

$$\frac{\partial \rho w}{\partial t} + \nabla.(\rho w \mathbf{U}) = -\frac{\partial P}{\partial z} + \nabla.(\mu\ \nabla w) - \frac{\partial\left(\rho \overline{u'w'}\right)}{\partial x} - \frac{\partial\left(\rho \overline{v'w'}\right)}{\partial y} - \frac{\partial\left(\rho \overline{w'^2}\right)}{\partial z} \quad (4)$$

$$\frac{\partial \rho E}{\partial t} + \nabla.(E \mathbf{U}) = \frac{\partial P}{\partial t} + \nabla.(\lambda \nabla T) + \nabla.\left(\rho \overline{u'h} + \rho \overline{v'h} + \rho \overline{w'h}\right) \quad (5)$$

The above equations are independently known as the continuity, x, y and z momentum, and energy equations respectively. In addition to the variables already clarified, *u'*, *v'*, *w'*, *h*, λ, *T* denote the x, y and z unsteady components of the velocity vector, enthalpy, thermal conductivity and static temperature respectively.

2.2 Turbulence Modelling

Turbulence modelling is a technique to close the above equations. This is achieved by accounting for the fluctuating velocity components *u'*, *v'*, and *w'* above. Relationships have been developed in order to make these fluctuating terms calculable as follows:

$$-\rho \overline{u'_i u'_j} = \mu_t E_{ij} = \mu_t \left(\frac{\partial U_i}{\partial x_j} + \frac{\partial U_j}{\partial x_i} \right) \quad (6)$$

$$\rho \overline{u'_i h} = \frac{\mu_t}{\mathrm{Pr}_t} \nabla h \quad (7)$$

In the two equations above an additional proportionality term is necessary. This is called the turbulent viscosity, μ_t. Two equation turbulence models calculate a value for this turbulent viscosity.

Popular turbulence models include the *k*–ε, *k*–ω and the SST model by Menter. The *k*–ε turbulence model is included below as it has been successfully implemented to give accurate results as shown in Section 5. The terms *k* and ε above denote the turbulent kinetic energy and its rate of dissipation respectively. The three equations below contain five adjustable constants, σ_k, σ_ε, $C_{1\varepsilon}$, $C_{1\varepsilon}$, C_μ, values of which have been established by comprehensive data fitting, and are fixed by the CFD software.

$$\frac{\partial \rho k}{\partial t} + \nabla.(\rho k \mathbf{U}) = \nabla.\left[\frac{\mu_t}{\sigma_k} \nabla k \right] + 2\mu_t E_{ij} \cdot E_{ij} - \rho \varepsilon \quad (8)$$

$$\frac{\partial \rho \varepsilon}{\partial t} + \nabla.(\rho \varepsilon \mathbf{U}) = \nabla.\left[\frac{\mu_t}{\sigma_\varepsilon} \nabla \varepsilon \right] - C_{2_\varepsilon} \rho \frac{\varepsilon^2}{k} + C_{1_\varepsilon} \frac{\varepsilon}{k} 2\mu_t E_{ij} \cdot E_{ij} \quad (9)$$

$$\mu_t = C \rho \theta \ell = \rho C_\mu \frac{k^2}{\varepsilon} \quad (10)$$

The CFD solver uses discretised forms of Equations (1 – 5), (8) and (9), and then solves them iteratively to calculate a converged solution for each variable at the nodes of elements created in a mesh of the flow domain of interest. This is not a trivial task and it is highly computationally intensive. However the benefits of this technique over traditional experimental techniques are that a clearer picture of what is happening internally within the RHVT can be obtained. This is in addition to the established theory outlined below.

3 RHVT Operation

3.1 Basic Operation

In a RHVT high pressure fluid, mainly compressed air, enters the tube and passes through nozzles achieving a high angular velocity and hence causing a vortex-type flow, as can be seen in Fig. 1. There are two outlets to the tube: the hot outlet is placed near the outer radius of the tube at the end away from the inlet nozzles and the cold outlet is placed at the centre of the tube at the same end as the air inlet.

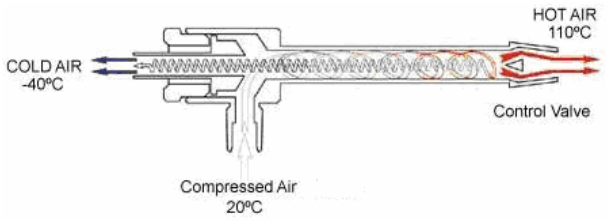

Fig. 1: Primary flow within the RHVT (courtesy of Exair Corporation).

By adjusting a control valve downstream of the hot outlet it is possible to vary the fraction of the incoming flow that leaves through the hot outlet on the periphery of the tube. The proportion of cold gas deflected back through the cold outlet is referred to as the cold fraction, μ_c,

$$\mu_c = \dot{m}_c / \dot{m}_{in} \quad (11)$$

where $\dot{m}_c$ and $\dot{m}_{in}$ are the cold and inlet mass flow rates respectively. By varying the cold fraction the hot and cold outlet temperatures can be adjusted.

The basic construction of the RHVT consists of a cylindrical tube, one or more tangential nozzles, and a throttle valve, as shown below.

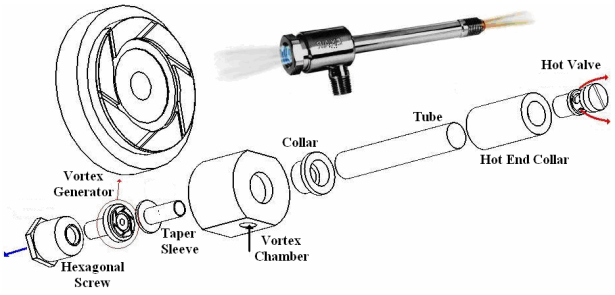

Fig. 2: Exploded view of a commercial RHVT, showing all components and highlighting the vortex generator.

3.2 Theory of Heat Migration

The longest serving and most established theory was first proposed by Hilsch [2]. He suggested that angular velocity gradients in the radial direction give rise to frictional coupling between different layers of the rotating flow resulting in a migration of energy via shear work from the inner layers to the outer layers. However this theory may not altogether explain the mode of heat transfer within the tube.

To supplement this theory a hypothesis has been forwarded by Ahlborn et al. [3, 4], that the presence of a secondary flow field contributes to the energy migration within the RHVT. This theory has since been supported by Gao et al. [5] and it is based on experimental evidence. Capturing this secondary flow and quantifying its influence using CFD is the main objective of this study.

3.3 Primary Flow within the RHVT

In a RHVT, when compressed gas is injected through tangential nozzles into its scroll chamber, a strong vortex flow field is established. The vortex flow field is comprised of a forced vortex near the centre and a free vortex at the periphery as shown below in Fig. 3. This type of flow field is maintained within the RHVT up to a stagnation point as highlighted. The stagnation point is defined as the location where the reversal in flow towards the cold outlet ends. It also marks the limiting point, whereby further increases of the vortex tube length beyond this point does not improve the energy separation, as observed by Aljuwayhel et al. [6]. This important aspect has been utilised in reducing the length of the computational domain of the vortex tube to that used by the experimental researchers. Towards the hot outlet the motion is no longer purely rotational due to friction from walls.

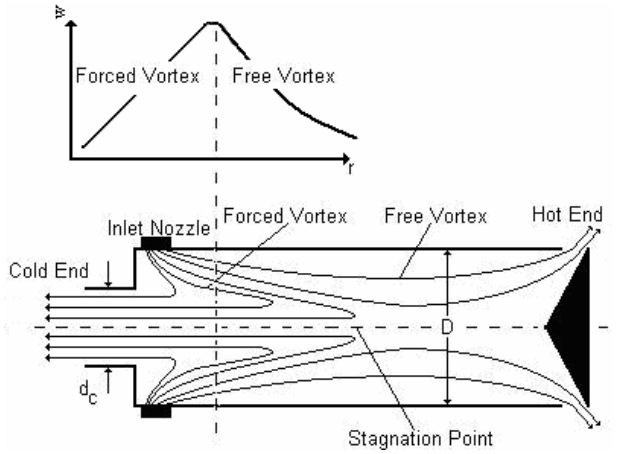

Fig. 3: Schematic flow pattern within the RHVT [7]. Also highlighted on top is the variation of tangential distribution with radial location in the inlet region of a vortex tube where a mixed forced vortex and free vortex are present.

3.4 Secondary Flow within the RHVT

A secondary flow field imbedded in the primary flow within the RHVT was discovered by Ahlborn et al. [3], see Fig. 4, when they measured the axial and tangential velocities in a vortex tube using a pitot tube. They discovered that the mass flow returning towards the cold outlet is much larger than the cold mass flow emerging out the cold end. In a following article Ahlborn et al. [4] went on to explain that the function of secondary flow within the RHVT is to provide a method of temperature separation based on the analogy of conventional heat pump mechanisms, as illustrated in Fig. 5. Although there is experimental evidence of a secondary flow within the RHVT, the analogy of its operation being similar to that of a heat pump contributing to the heat migration is still open to question.

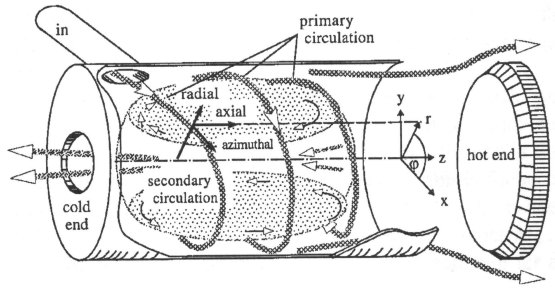

Fig. 4: Primary and secondary flows within the RHVT [3].

By capturing this secondary flow through the use of CFD, a clearer insight can be gained. A greater foundation for this theory can be quantified if evidence of the heat pump cycle of expansion, heat

rejection, compression and energy absorption can be detected.

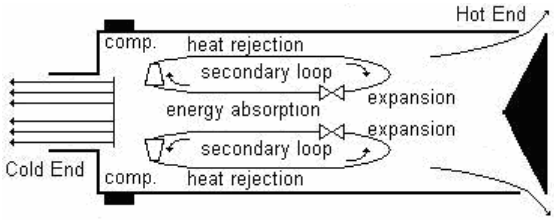

Fig. 5: Hypothesised refrigeration cycle within a RHVT, adapted from [4].

3.5 Previous CFD Studies

Previous CFD studies of the RHVT have been carried out by researchers such as Aljuwayhel et al. [6], Behera et al. [7], Skye et al. [8]. and Frohlingsdorf et al. [9]

Only Behera et al. [7] have previously published literature on a RHVT using a complete three dimensional vortex tube. Most researchers have simplified the analysis to either two dimensional models or three dimensional partial sectors of the flow. This analysis is the first study focusing on secondary flow within the RHVT. All previous studies have been small scale parametric studies, and although Behera et al. [7] have successfully captured secondary flow, they have not tried to suggest its thermodynamic influence.

4 RHVT CFD Model

Shown above in Fig. 2 are the components that comprise the RHVT. However, for CFD analysis, this complicated shape can be resolved down to a very simple basic shape without loss of the most important aspects of the device. From the exploded view of a commercial vortex tube in Fig. 2 the only elements required are

- A cylindrical tube
- A vortex generator at the entrance plane
- A central hole for the cold outlet
- An outlet on the periphery of the tube for the hot outlet

These requirements have resulted in the basic shape shown below for analysis by the CFD software. The geometry of this RHVT follows that of the size used by the experimental researchers, Promvonge et al. [10] and Soni [11], whose comparative results are used in the mesh convergence study shown in Fig. 7 in Section 5.1. However the length of the tube has been shortened considerably as previously stated in Section 3.2. This shortening saves a considerable amount of computational effort, both memory wise and CPU processing time.

The elongated cold outlet has been included because of the secondary flow in the RHVT. If the cold outlet was placed on the main body of the RHVT, it could cause significant problems for any outlet boundary condition specified, as secondary flow may recirculate at the outlet. Thus any flow trying to re-enter the domain would affect the solution considerably. Also as can be seen below the vortex generator has been simplified by only including the relevant nozzles.

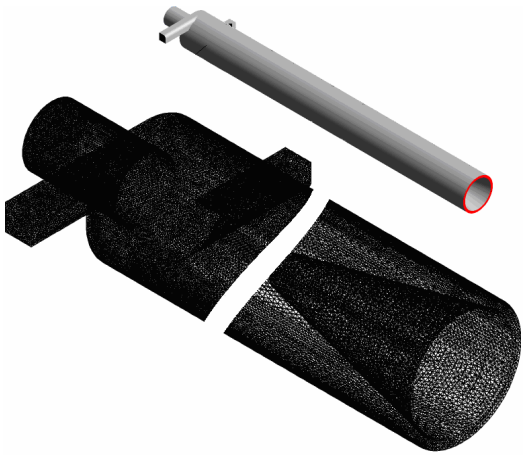

Fig. 6: CFD model of the 3D RHVT with two inlet nozzles, also shown is an example of the unstructured mesh at the inlet nozzles, cold outlet and the conical hot outlet.

4.1 Boundary Conditions

Within the CFD model it is the boundary conditions that give the computational model the required flow characteristics of the RHVT. Previous publications have successfully implemented total pressure and static temperature at the inlet nozzles along with static pressures at the outlets as boundary conditions [6 – 8]. However to implement these conditions, the total pressure at the inlet must be calculated and as a result a sufficient static pressure drop through the RHVT may not occur. This is because the total pressure specification at the inlet is proportioned out as both static and dynamic pressure and this may mean an insufficient static pressure drop is calculated by the CFD solver.

Importantly, experimental researchers record information regarding the gauge pressure and total temperature at the inlet. It would appear that these recorded values appear to be the most useful boundary conditions at this location. Significantly the temperature at the outlets of the RHVT published by these researchers is the total/stagnation temperature of the fluid. This is because the temperature measurement probe creates a stagnation point in the high speed air flow, as also

concluded by Skye et al. [8]. The resulting boundary conditions are as follows:

4.1.1 Nozzle Inlet

The static pressure was set to 2 Bar gauge along with a total temperature of 296.5 K at the inlet. The total temperature used at the inlet provides a basis for calculating and limiting the mass flow through the domain.

4.1.2 Cold Outlet

The static pressure at the cold outlet was set to atmospheric pressure as this outlet is open to the atmosphere.

4.1.3 Hot Outlet

The static pressure at the hot outlet was set to 0.5 Bar gauge. This was in order to obtain a cold fraction, $\mu_c \approx 0.4$, as required in order to compare predicted and experimental results in Section 5. The pressure at the hot outlet of the computational domain is always above atmospheric. This is because the hot valve in an actual RHVT serves to increase the back pressure at the peripheral outlet before the valve which is where the computational outlet is located.

5 Results

5.1 Mesh Convergence Study

A mesh convergence study was conducted focusing on both the static and total temperature outputs of the RHVT, the results of which are shown below.

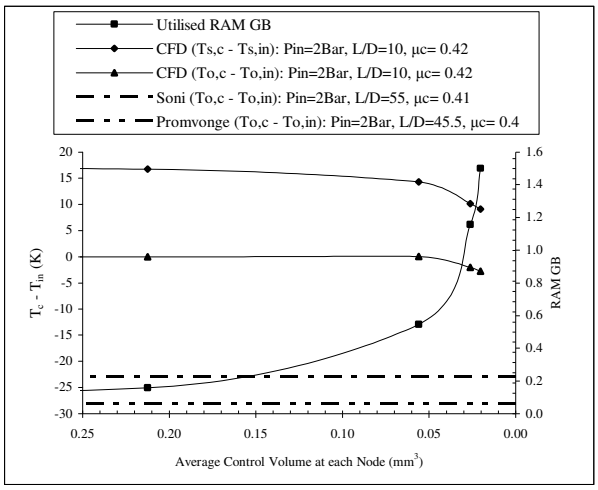

Fig. 7: CFD mesh convergence study for a RHVT similar to [10] and [11]. The graph shows the variance of the cold outlet total temperature drop ($T_{o,c} - T_{in,c}$) and cold static temperature difference ($T_{s,c} - T_{in,c}$) versus the mesh density in the form of the average control volume at each node. The targeted computed total temperature drop from the experimental results of [10 - 11] is highlighted along with the utilised RAM required for each mesh solver run.

As can the been the a total temperature drop ($T_{o,c} - T_{in,c}$) at the cold outlet in the computational RHVT, has developed at quite high mesh densities, but has not yet reached the target temperature drops specified by the experimental results from [10-11].

5.2 Temperature Contour Plot

The most recent total temperature contour plot along the central axis of the RHVT is shown below as an example of the current total temperature distribution captured within the tube.

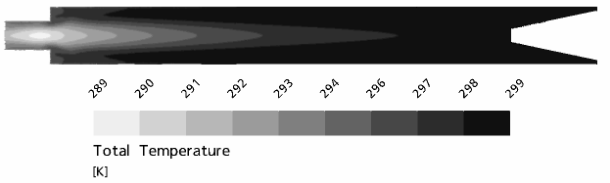

Fig. 8: Total temperature contour plot along the central axis of the RHVT, for μ_c=0.4, P_{in}=2Bar, L/D=10.

5.3 Velocity Profiles

Internal velocity profiles have been compared to the experimental results published by Gao et al. [5], as their results are, to the best of the authors knowledge, the most recent and comprehensive results published for both tangential and axial velocities. The experimental results are non-dimensionalised and can therefore be compared to results from similar RHVT as is the case below. The comparison between measured and predicted normalised velocity distributions shown below is very encouraging.

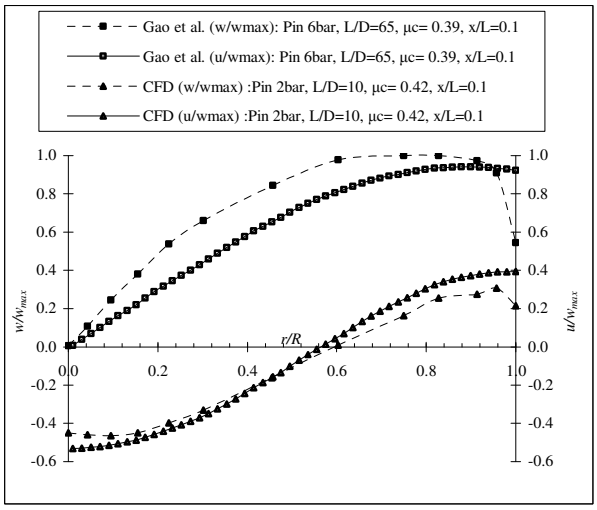

Fig. 9: Comparison of the computed variation of internal normalised tangential and axial velocities at normalised radial locations with experimental results from [5] at the inlet region within the RHVT.

5.4 Streamline Plot

The two dimensional streamline plot below shows a distinct relationship to that expected from the theory outlined in Fig. 3. Significantly a region of

recirculating secondary flow has been captured and is highlighted along with the stagnation point location.

Fig. 10: Predicted streamline plot along the central axis show a successfully captured secondary flow within the RHVT, for μ_c=0.4, P_{in}=2Bar, L/D=10.

6 Conclusion

The mesh convergence study shown above is ongoing and is expected to be completed in the near future. The current results of the computed total temperature drop at the cold outlet are progressing towards the targeted experimental results and this advancement will in time be complete.

This computational study of the RHVT has shown that CFD techniques are well suited to analysing the highly complex flows contained within the RHVT. The computed flow fields compare favourably to previous experimental results and show the following:

- A mixed forced and free vortex at the entrance region.
- Positive and negative axial flow at the entrance region.
- A stagnation point location.
- The presence of secondary flow.

Although a secondary flow has proven to be present its contribution to the mode of heat migration is not fully substantiated.

Acknowledgements:
This study has been funded by the Dept. of Mechanical Engineering, DIT, and also by the Embark Initiative managed by the IRCSET as part of the National Development Plan, Ireland 2000 - 2006.

References:

[1] Fulton, C.D., Ranque's Tube, *Journal of the American Society of Refrigeration Engineering*, Vol. 5, 1950, pp. 473-479.

[2] Hilsch, R., The Use of the Expansion of Gases in a Centrifugal Field as a Cooling Process, *Review of Scientific Instruments*, Vol. 18, No. 2, 1947, pp. 108-113.

[3] Ahlborn, B. and Groves, S., Secondary Flow in a Vortex Tube, *Fluid Dynamics Research*, Vol. 21, 1997, pp. 73-86.

[4] Ahlborn, B. and Gordon, J.M., The Vortex Tube as a Classic Thermodynamic Refrigeration Cycle, *Journal of Applied Physics*, Vol. 88, No. 6, 2000, pp. 3645-3653.

[5] Gao, C. M., Bosschaart, K. J., Zeegers, J. C. H., and de Waele, A.T.A.M., Experimental Study on a Simple RHVT, *Cryogenics*, Vol. 45, 2005, pp. 173-183.

[6] Aljuwayhel, N. F., Nellis, G. F., and Klein, S. A., Parametric and Internal Study of the Vortex Tube using a CFD Model, *International Journal of Refrigeration*, Vol.28, 2005, pp. 442-450.

[7] Behera, U., and Paul, P. J., CFD Analysis and Experimental Investigations towards Optimizing the Parameters of RHVT, *International Journal of Heat and Mass Transfer*, Vol.48, 2005, pp. 1961-1973.

[8] Skye, H. M., Nellis, G. F., and Klein, S. A., Comparison of CFD Analysis to Empirical Data in a Commercial Vortex Tube, *International Journal of Refrigeration*, Vol.29, 2006, pp. 71-80.

[9] Frohlingsdorf, W. and Unger, H., Numerical Investigation of the Compressible Flow and the Energy Separation in the RHVT, *International Journal of Heat and Mass Transfer*, Vol. 42, 1999, pp.415-422.

[10] Promvonge, P. and Eiamsa-ard, S., Investigation of the Thermal Separation in a Vortex Tube Refrigerator, *Science Asia*, Vol. 31, 2005, pp. 215-223.

[11] Soni, Y., *A Parametric Study of the Ranque-Hilsch Tube*, University of Idaho, 1973.